Science Advances
AAAS

advances.sciencemag.org/cgi/content/full/6/26/eabb8133/DC1

Supplementary Materials for

Transient stealth coating of liver sinusoidal wall by anchoring two-armed PEG for retargeting nanomedicines

Anjaneyulu Dirisala, Satoshi Uchida*, Kazuko Toh, Junjie Li, Shigehito Osawa, Theofilus A. Tockary, Xueying Liu, Saed Abbasi, Kotaro Hayashi, Yuki Mochida, Shigeto Fukushima, Hiroaki Kinoh, Kensuke Osada, Kazunori Kataoka*

*Corresponding author. Email: suchida@bmw.t.u-tokyo.ac.jp (S.U.); kataoka@ifi.u-tokyo.ac.jp (K.K.)

Published 26 June 2020, *Sci. Adv.* **6**, eabb8133 (2020)
DOI: 10.1126/sciadv.abb8133

The PDF file includes:

Other Supplementary Material for this manuscript includes the following:

(available at advances.sciencemag.org/cgi/content/full/6/26/eabb8133/DC1)

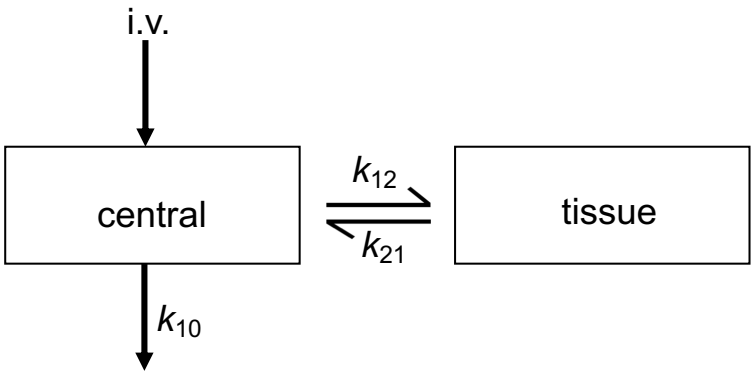

Supplementary Figure S1. Two compartment model. In this model, polymers are intravenously (i.v.) injected to blood circulation, which is defined as a central compartment. From the compartment, polymers translocate to a tissue compartment, which includes the liver sinusoid, at a rate constant of k_{12}, and then are back to the central compartment at a rate constant of k_{21}. Polymers in a central compartment are eventually excreted at a rate constant of k_{10}. The result of pharmacokinetic analyses is shown in **Table S1**.

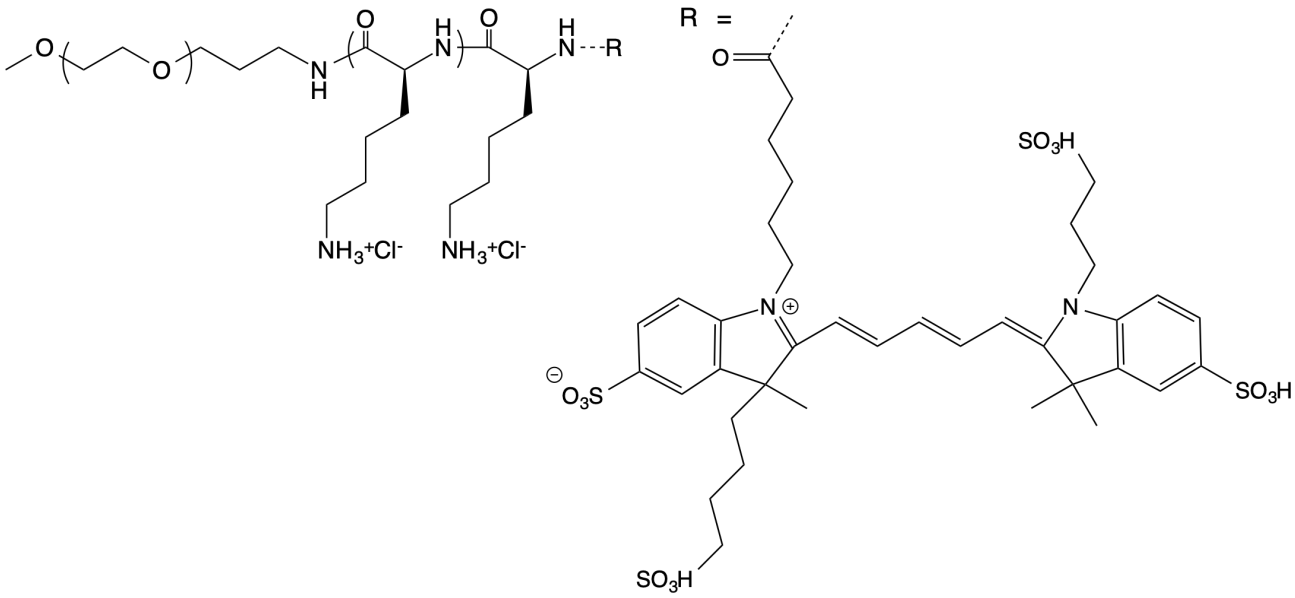

Supplementary Figure S2. Alexa 647-labelled 1-arm-PEG-OligoLys.

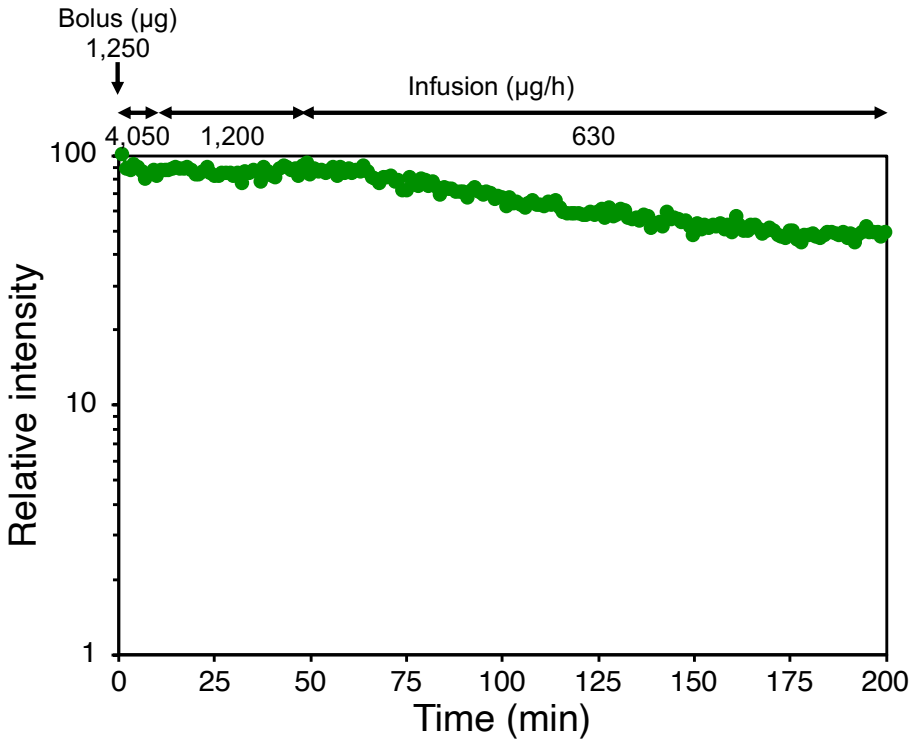

Supplementary Figure S3. Blood clearance profile of 2-arm-PEG−OligoLys under intravenous infusion. Bolus intravenous injection of Alexa594-labelled 2-arm-PEG−OligoLys was performed at a dose of 1,250 μg/mouse, which is the same as that used throughout this study, followed by its infusion with varying rate in a stepwise manner as follows: 4,050 μg/h/mouse (0-10 min), 1,200 μg/h/mouse (10-50 min), and 630 μg/h/mouse. Fluorescence intensity of a vessel in the earlobe was observed using intravital confocal microscopy.

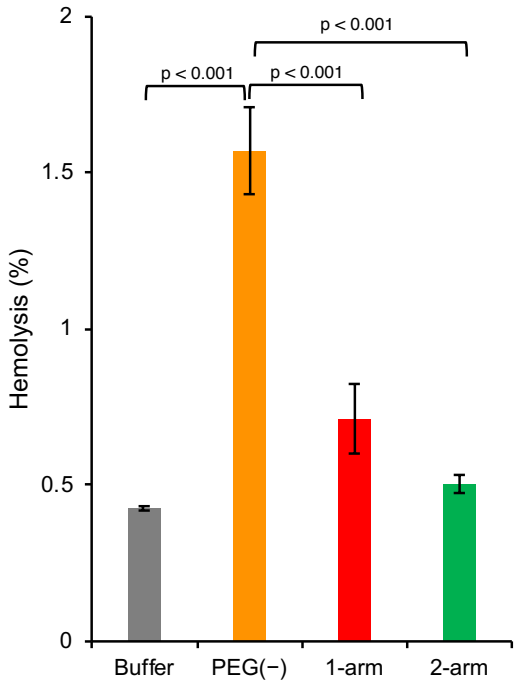

Supplementary Figure S4. *Ex vivo* hemolysis assay. Mouse red blood cells were incubated with PBS (buffer), non-PEGylated OligoLys (PEG(−)), 1-arm-PEG−OligoLys (1-arm) and 2-arm-PEG−OligoLys (2-arm) for 1 h at 37 °C. Release of hemoglobin was spectroscopically quantified. n = 4. Statistical analysis was performed using analysis of variance (ANOVA) followed by Tukey's test.

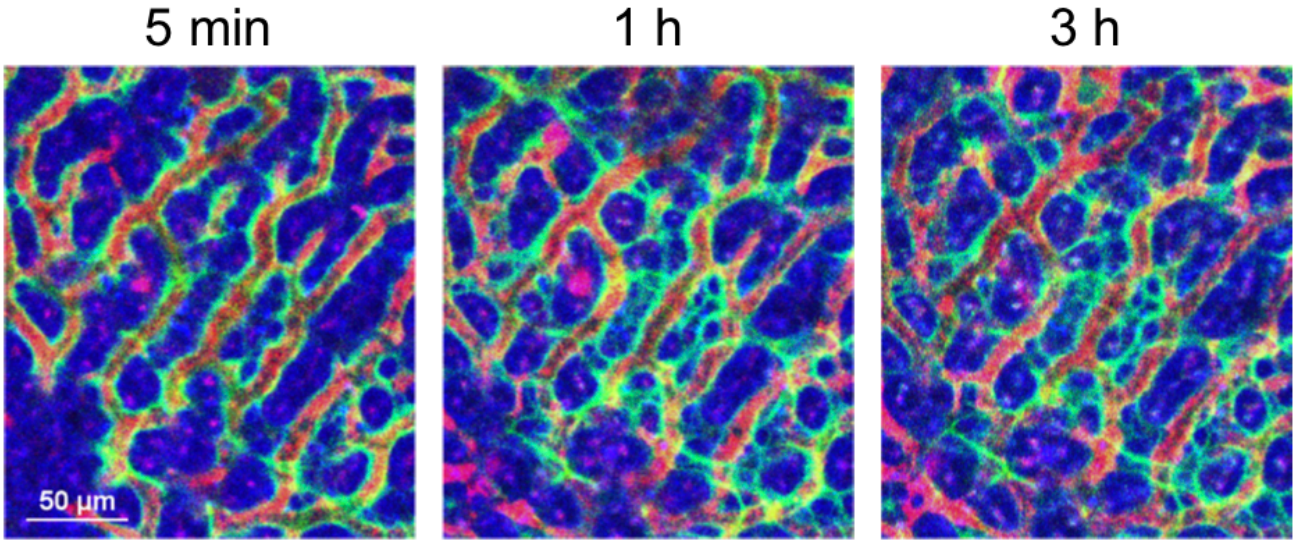

Supplementary Figure S5. Inhibition of sinusoidal clearance of polyplex micelle by pre-injection of 2-arm-PEG−OligoLys. Alexa594-labelled 2-arm-PEG−OligoLys (green) was intravenously injected to coat liver sinusoidal wall with PEG, followed by the intravenous injection of polyplex micelle loading Cy5-labelled pDNA (red) 5 min later. IVCLSM images of the liver was obtained 5 min, 1 h and 3 h after PM injection. Blue: autofluorescence of liver parenchyma.

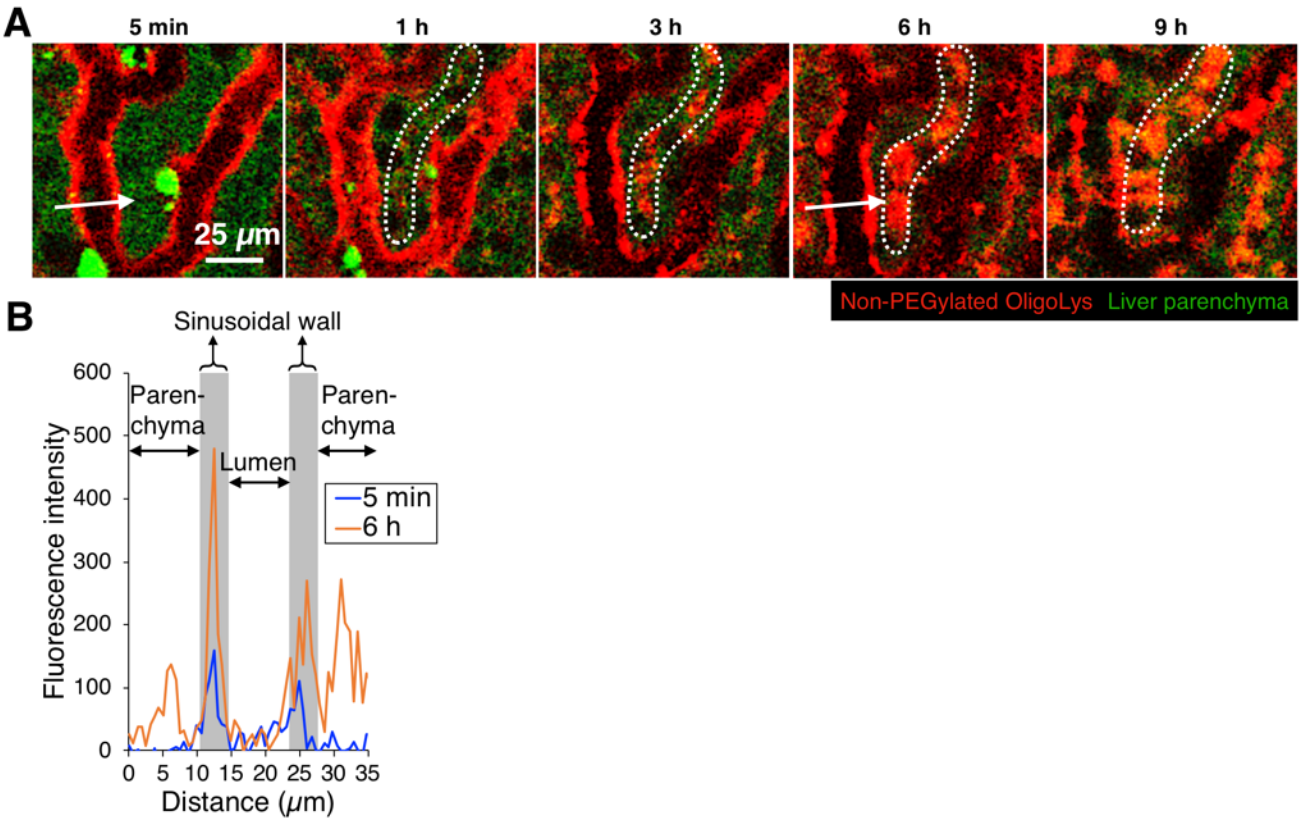

Supplementary Figure S6. Distribution of non-PEGylated OligoLys in the liver. (**A**) IVCLSM images of the liver after intravenous injection of Alexa594-labelled non-PEGylated OligoLys. Presumable regions of bile canaliculi are encircled with white dotted lines. (**B**) Intensity profile of Alexa594 in the white arrows shown in (**A**).

Supplementary Table S1. Pharmacokinetic analysis.

	PEG without OligoLys	1-arm-PEG−OligoLys	2-arm-PEG−OligoLys
Model	1-compartment	2-compartment	2-compartment
Distribution phase half-life ($t_{1/2\alpha}$)		0.24 h (14.4 min)	0.27 h (16.4 min)
Elimination phase half-life ($t_{1/2\beta}$)	19.8 h	13.3 h	5.7 h
k_{10}*		0.11 h^{-1}	0.54 h^{-1}
k_{12}*		1.48 h^{-1}	1.55 h^{-1}
k_{21}*		1.35 h^{-1}	0.57 h^{-1}
R^2	0.83	0.90	0.98

* See **Fig. S1** for the definition of these values.

Supplementary Table S2. Blood examination.

	Buffer	Non-PEGylated OligoLys	1-arm-PEG−OligoLys	2-arm-PEG−OligoLys
LDH	243.7 ± 75.3	400.0 ± 66.4**	245.4 ± 37.0	254.6 ± 68.3
AST	73.3 ± 18.8	69 ± 11.1	82.3 ± 30.4	83 ± 16.7
ALT	76.8 ± 33.7	56.8 ± 13.7	85 ± 35.9	91.7 ± 30.9
BUN	20.8 ± 2.2	22 ± 1.6	19.9 ± 0.5	18.3 ± 2.2
CRE	0.1 ± 0.0	0.1 ± 0.0	0.1 ± 0.0	0.1 ± 0.0

Data are shown as mean ± standard error of the mean. $n = 4$. Statistical analyses were performed using analysis of variance (ANOVA) followed by Tukey's test. ** $p < 0.01$ vs. Buffer.

Abbreviations: LDH: lactate dehydrogenase, AST: aspartate transaminase, ALT: alanine transaminase, BUN: blood urea nitrogen, CRE: creatinine

Supplementary Note S1 Mathematical modelling of endocytosis of 1- and 2-arm-PEG−OligoLys.

1- and 2-arm-PEG−OligoLys is assumed as 1 sphere of 80-kDa PEG and 2 spheres of 40-kDa PEG, respectively. Radius of each PEG chain (r_p) is set to radius of gyration (R_g), 14 nm for 80-kDa PEG, 9.4 nm for 40-kDa, respectively, based on the calculation by the equation, $R_g = 0.181 \times (M_n \text{ of PEG} / 44.06)^{0.58}$ (in nm) (*52*). The PEG spheres are first placed onto sinusoidal cell membrane in a hexagonal lattice structure with each sphere circumscribed with surrounding spheres, without overlapping (**Fig. S7A**). In endocytosis, curving of cell membrane induces the overlapping between adjacent PEG chains attached to the membrane (**Fig. S7B**). Endocytotic vesicle is assumed as a sphere with radius of r_e and diameter of d_e. In this model, distance between 2 adjacent PEG spheres (a) is calculated by a following equation.

$$a = 2 \times (r_e - r_p) \times \sin(r_p/r_e)$$

Using this value, overlapping volume of 2 adjacent PEG spheres (V_a) is calculated by a following equation.

$$V_a = 4/3 \times \pi \times {r_p}^3 - \pi \times a \times {r_p}^2 + 1/12 \times \pi \times a^3$$

One PEG sphere has 6 adjacent PEG spheres with each overlapping volume (V_a) shared by 2 PEG spheres. Thus, overlapping volume per each PEG sphere (V_b) is calculated by a following equation.

$$V_b = 3 \times V_a$$

Each PEG sphere occupies cell membrane with area of $3\sqrt{3}/2 \times r_p$. Thus, overlapping volume per unit membrane area (V) is calculated by a following equation.

$$V = V_b / (3\sqrt{3}/2 \times r_p)$$

V is plotted against the diameter of endocytotic vesicle (d_e) for each of 1- and 2-arm-PEG−OligoLys (V_{80k} and V_{40k}, respectively), in **Fig. S7C**. In addition, ratio of V_{80k} to V_{40k} is plotted against d_e, in **Fig. S7D**. While V decreases with increase in d_e, overlapping volume of 80-kDa PEG is more than 3-fold higher than that of 40-kDa PEG in the d_e range from 50 nm to 200 nm.

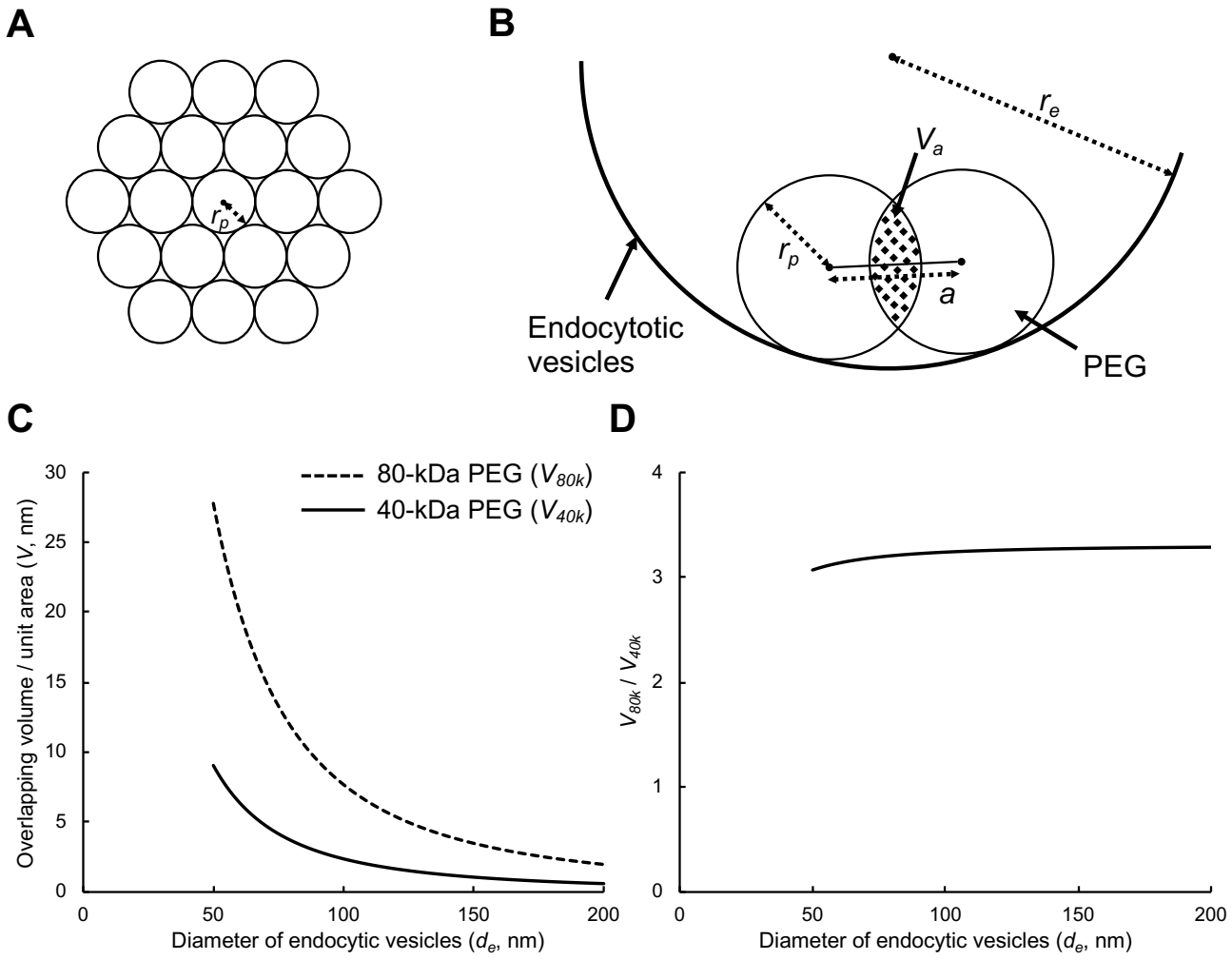

Supplementary Figure S7. Mathematical modelling of endocytosis of 1- and 2-arm-PEG−OligoLys. (**A**) PEG spheres placed onto cell membrane in a hexagonal lattice structure with each sphere circumscribed with surrounding spheres, without overlapping. (**B**) Calculation of the overlapping volume between adjacent PEG chains after endocytosis. (**C**) The overlapping volume between adjacent PEG chains per unit membrane area (V). (**D**) Ratio of V of 80-kDa PEG (V_{80k}) to V of 40-kDa PEG (V_{40k}).

Supplementary Movies

Supplementary Movie S1. IVCLSM observation of the liver after co-injection of 1- and 2-arm-PEG−OligoLys. Red: Alexa647-labelled 1-arm-PEG−OligoLys, Green: Alexa594-labelled 2-arm-PEG−OligoLys.

Supplementary Movie S2. IVCLSM observation of the liver after sequential injection of 2-arm-PEG−OligoLys and PM. Five minutes after intravenous injection of Alexa594-labelled 2-arm-PEG−OligoLys (green), polyplex micelle (PM) loading Cy5-labelled pDNA (red) was intravenously injected. Blue: autofluorescence of liver parenchyma.

REFERENCES AND NOTES

1. M. E. Davis, Z. G. Chen, D. M. Shin, Nanoparticle therapeutics: An emerging treatment modality for cancer. *Nat. Rev. Drug Discov.* **7**, 771–782 (2008).

2. T. Lammers, S. Aime, W. E. Hennink, G. Storm, F. Kiessling, Theranostic nanomedicine. *Acc. Chem. Res.* **44**, 1029–1038 (2011).

3. S. Mura, J. Nicolas, P. Couvreur, Stimuli-responsive nanocarriers for drug delivery. *Nat. Mater.* **12**, 991–1003 (2013).

4. V. J. Yao, S. D'Angelo, K. S. Butler, C. Theron, T. L. Smith, S. Marchiò, J. G. Gelovani, R. L. Sidman, A. S. Dobroff, C. J. Brinker, A. R. M. Bradbury, W. Arap, R. Pasqualini, Ligand-targeted theranostic nanomedicines against cancer. *J. Control. Release* **240**, 267–286 (2016).

5. B. Pelaz, C. Alexiou, R. A. Alvarez-Puebla, F. Alves, A. M. Andrews, S. Ashraf, L. P. Balogh, L. Ballerini, A. Bestetti, C. Brendel, S. Bosi, M. Carril, W. C. W. Chan, C. Chen, X. Chen, X. Chen, Z. Cheng, D. Cui, J. Du, C. Dullin, A. Escudero, N. Feliu, M. Gao, M. George, Y. Gogotsi, A. Grünweller, Z. Gu, N. J. Halas, N. Hampp, R. K. Hartmann, M. C. Hersam, P. Hunziker, J. Jian, X. Jiang, P. Jungebluth, P. Kadhiresan, K. Kataoka, A. Khademhosseini, J. Kopeček, N. A. Kotov, H. F. Krug, D. S. Lee, C.-M. Lehr, K. W. Leong, X.-J. Liang, M. L. Lim, L. M. Liz-Marzán, X. Ma, P. Macchiarini, H. Meng, H. Möhwald, P. Mulvaney, A. E. Nel, S. Nie, P. Nordlander, T. Okano, J. Oliveira, T. H. Park, R. M. Penner, M. Prato, V. Puntes, V. M. Rotello, A. Samarakoon, R. E. Schaak, Y. Shen, S. Sjöqvist, A. G. Skirtach, M. G. Soliman, M. M. Stevens, H.-W. Sung, B. Z. Tang, R. Tietze, B. N. Udugama, J. S. VanEpps, T. Weil, P. S. Weiss, I. Willner, Y. Wu, L. Yang, Z. Yue, Q. Zhang, Q. Zhang, X.-E. Zhang, Y. Zhao, X. Zhou, W. J. Parak, Diverse applications of nanomedicine. *ACS Nano* **11**, 2313–2381 (2017).

6. H. Cabral, K. Miyata, K. Osada, K. Kataoka, Block copolymer micelles in nanomedicine applications. *Chem. Rev.* **118**, 6844–6892 (2018).

7. D. E. Owens III, N. A. Peppas, Opsonization, biodistribution, and pharmacokinetics of polymeric nanoparticles. *Int. J. Pharm.* **307**, 93–102 (2006).

8. B. Wang, X. He, Z. Zhang, Y. Zhao, W. Feng, Metabolism of nanomaterials in vivo: Blood circulation and organ clearance. *Acc. Chem. Res.* **46**, 761–769 (2013).

9. K. M. Tsoi, S. A. MacParland, X.-Z. Ma, V. N. Spetzler, J. Echeverri, B. Ouyang, S. M. Fadel, E. A. Sykes, N. Goldaracena, J. M. Kaths, J. B. Conneely, B. A. Alman, M. Selzner, M. A. Ostrowski, O. A. Adeyi, A. Zilman, I. D. McGilvray, W. C. W. Chan, Mechanism of hard-nanomaterial clearance by the liver. *Nat. Mater.* **15**, 1212–1221 (2016).

10. G. Wang, D. Simberg, Role of scavenger receptors in immune recognition and targeting of nanoparticles. *Rev. Cell Biol. Mol. Med.* **1**, 166–189 (2006).

11. K. K. Sørensen, J. Simon-Santamaria, R. S. McCuskey, B. Smedsrød, Liver sinusoidal endothelial cells. *Compr. Physiol.* **5**, 1751–1774 (2015).

12. F. Campbell, F. L. Bos, S. Sieber, G. Arias-Alpizar, B. E. Koch, J. Huwyler, A. Kros, J. Bussmann, Directing nanoparticle biodistribution through evasion and exploitation of stab2-dependent nanoparticle uptake. *ACS Nano* **12**, 2138–2150 (2018).

13. F. Jacobs, E. Wisse, B. De Geest, The role of liver sinusoidal cells in hepatocyte-directed gene transfer. *Am. J. Pathol.* **176**, 14–21 (2010).

14. L. P. Ganesan, S. Mohanty, J. Kim, K. R. Clark, J. M. Robinson, C. L. Anderson, Rapid and efficient clearance of blood-borne virus by liver sinusoidal endothelium. *PLOS Pathog.* **7**, e1002281 (2011).

15. K. Kataoka, A. Harada, Y. Nagasaki, Block copolymer micelles for drug delivery: Design, characterization and biological significance. *Adv. Drug Deliv. Rev.* **47**, 113–131 (2001).

16. A. Soundararajan, A. Bao, W. T. Phillips, R. Perez III, B. A. Goins, [^{186}Re]Liposomal doxorubicin (Doxil): In vitro stability, pharmacokinetics, imaging and biodistribution in a head and neck squamous cell carcinoma xenograft model. *Nucl. Med. Biol.* **36**, 515–524 (2009).

17. J. A. MacKay, M. Chen, J. R. McDaniel, W. Liu, A. J. Simnick, A. Chilkoti, Self-assembling chimeric polypeptide-doxorubicin conjugate nanoparticles that abolish tumours after a single injection. *Nat. Mater.* **8**, 993–999 (2009).

18. Y. Anraku, A. Kishimura, A. Kobayashi, M. Oba, K. Kataoka, Size-controlled long-circulating PICsome as a ruler to measure critical cut-off disposition size into normal and tumor tissues. *Chem. Commun.* **47**, 6054–6056 (2011).

19. M. Ogris, S. Brunner, S. Schüller, R. Kircheis, E. Wagner, PEGylated DNA/transferrin-PEI complexes: Reduced interaction with blood components, extended circulation in blood and potential for systemic gene delivery. *Gene Ther.* **6**, 595–605 (1999).

20. T. Merdan, K. Kunath, H. Petersen, U. Bakowsky, K. H. Voigt, J. Kopecek, T. Kissel, PEGylation of poly(ethylene imine) affects stability of complexes with plasmid DNA under in vivo conditions in a dose-dependent manner after intravenous injection into mice. *Bioconjug. Chem.* **16**, 785–792 (2005).

21. J.-M. Prill, V. Subr, N. Pasquarelli, T. Engler, A. Hoffmeister, S. Kochanek, K. Ulbrich, F. Kreppel, Traceless bioresponsive shielding of adenovirus hexon with HPMA copolymers maintains transduction capacity in vitro and in vivo. *PLOS One* **9**, e82716 (2014).

22. L. Krutzke, J. M. Prill, T. Engler, C. Q. Schmidt, Z. Xu, A. P. Byrnes, T. Simmet, F. Kreppel, Substitution of blood coagulation factor X-binding to Ad5 by position-specific PEGylation: Preventing vector clearance and preserving infectivity. *J. Control. Release* **235**, 379–392 (2016).

23. M. R. A. Abdollah, T. J. Carter, C. Jones, T. L. Kalber, V. Rajkumar, B. Tolner, C. Gruettner, M. Zaw-Thin, J. Baguña Torres, M. Ellis, M. Robson, R. B. Pedley, P. Mulholland, R. T. M. de Rosales, K. A. Chester, Fucoidan prolongs the circulation time of dextran-coated iron oxide nanoparticles. *ACS Nano* **12**, 1156–1169 (2018).

24. H. J. Haisma, J. A. A. M. Kamps, G. K. Kamps, J. A. Plantinga, M. G. Rots, A. R. Bellu, Polyinosinic acid enhances delivery of adenovirus vectors in vivo by preventing sequestration in liver macrophages. *J. Gen. Virol.* **89**, 1097–1105 (2008).

25. M. R. A. Abdollah, T. Kalber, B. Tolner, P. Southern, J. C. Bear, M. Robson, R. B. Pedley, I. P. Parkin, Q. A. Pankhurst, P. Mulholland, K. Chester, Prolonging the circulatory retention of SPIONs using dextran sulfate: In vivo tracking achieved by functionalisation with near-infrared dyes. *Faraday Discuss.* **175**, 41–58 (2014).

26. R. J. Allen, B. Mathew, K. G. Rice, PEG-peptide inhibition of scavenger receptor uptake of nanoparticles by the liver. *Mol. Pharm.* **15**, 3881–3891 (2018).

27. X. Sun, X. Yan, O. Jacobson, W. Sun, Z. Wang, X. Tong, Y. Xia, D. Ling, X. Chen, Improved tumor uptake by optimizing liposome based RES blockade strategy. *Theranostics* **7**, 319–328 (2017).

28. Z. Xu, J. Tian, J. S. Smith, A. P. Byrnes, Clearance of adenovirus by Kupffer cells is mediated by scavenger receptors, natural antibodies, and complement. *J. Virol.* **82**, 11705–11713 (2008).

29. S. Alidori, R. L. Bowman, D. Yarilin, Y. Romin, A. Barlas, J. J. Mulvey, S. Fujisawa, K. Xu, A. Ruggiero, V. Riabov, D. L. J. Thorek, H. D. S. Ulmert, E. J. Brea, K. Behling, J. Kzhyshkowska, K. Manova-Todorova, D. A. Scheinberg, M. R. McDevitt, Deconvoluting hepatic processing of carbon nanotubes. *Nat. Commun.* **7**, 12343 (2016).

30. H. Y. Hsu, S. L. Chiu, M. H. Wen, K. Y. Chen, K. F. Hua, Ligands of macrophage scavenger receptor induce cytokine expression via differential modulation of protein kinase signaling pathways. *J. Biol. Chem.* **276**, 28719–28730 (2001).

31. S. Marshall-Clarke, J. E. Downes, I. R. Haga, A. G. Bowie, P. Borrow, J. L. Pennock, R. K. Grencis, P. Rothwell, Polyinosinic acid is a ligand for toll-like receptor 3. *J. Biol. Chem.* **282**, 24759–24766 (2007).

32. K. Walton, Experiments with dextran sulphate as an anticoagulant. *Proc. R. Soc. Med.* **44**, 563–564 (1951).

33. J. L. Stow, L. Kjéllen, E. Unger, M. Höök, M. G. Farquhar, Heparan sulfate proteoglycans are concentrated on the sinusoidal plasmalemmal domain and in intracellular organelles of hepatocytes. *J. Cell Biol.* **100**, 975–980 (1985).

34. R. S. Burke, S. H. Pun, Extracellular barriers to in vivo PEI and PEGylated PEI polyplex-mediated gene delivery to the liver. *Bioconjug. Chem.* **19**, 693–704 (2008).

35. Z. Kadlecova, L. Baldi, D. Hacker, F. M. Wurm, H.-A. Klok, Comparative study on the in vitro cytotoxicity of linear, dendritic, and hyperbranched polylysine analogues. *Biomacromolecules* **13**, 3127–3137 (2012).

36. M. A. Gosselin, W. Guo, R. J. Lee, Efficient gene transfer using reversibly cross-linked low molecular weight polyethylenimine. *Bioconjug. Chem.* **12**, 989–994 (2001).

37. T. Yamaoka, Y. Tabata, Y. Ikada, Distribution and tissue uptake of poly(ethylene glycol) with different molecular weights after intravenous administration to mice. *J. Pharm. Sci.* **83**, 601–606 (1994).

38. J. W. Smit, A. H. Schinkel, B. Weert, D. K. F. Meijer, Hepatobiliary and intestinal clearance of amphiphilic cationic drugs in mice in which both *mdr1a* and *mdr1b* genes have been disrupted. *Br. J. Pharmacol.* **124**, 416–424 (1998).

39. K. Miyata, Y. Kakizawa, N. Nishiyama, A. Harada, Y. Yamasaki, H. Koyama, K. Kataoka, Block catiomer polyplexes with regulated densities of charge and disulfide cross-linking directed to enhance gene expression. *J. Am. Chem. Soc.* **126**, 2355–2361 (2004).

40. K. M. Takeda, Y. Yamasaki, A. Dirisala, S. Ikeda, T. A. Tockary, K. Toh, K. Osada, K. Kataoka, Effect of shear stress on structure and function of polyplex micelles from poly(ethylene glycol)-poly(L-lysine) block copolymers as systemic gene delivery carrier. *Biomaterials* **126**, 31–38 (2017).

41. M. Oba, Y. Vachutinsky, K. Miyata, M. R. Kano, S. Ikeda, N. Nishiyama, K. Itaka, K. Miyazono, H. Koyama, K. Kataoka, Antiangiogenic gene therapy of solid tumor by systemic injection of polyplex micelles loading plasmid DNA encoding soluble Flt-1. *Mol. Pharm.* **7**, 501–509 (2010).

42. Y. Vachutinsky, M. Oba, K. Miyata, S. Hiki, M. R. Kano, N. Nishiyama, H. Koyama, K. Miyazono, K. Kataoka, Antiangiogenic gene therapy of experimental pancreatic tumor by sFlt-1 plasmid DNA carried by RGD-modified crosslinked polyplex micelles. *J. Control. Release* **149**, 51–57 (2011).

43. C. Hinderer, N. Katz, E. L. Buza, C. Dyer, T. Goode, P. Bell, L. K. Richman, J. M. Wilson, Severe toxicity in nonhuman primates and piglets following high-dose intravenous administration of an adeno-associated virus vector expressing human SMN. *Hum. Gene Ther.* **29**, 285–298 (2018).

44. Z. Wang, T. Zhu, C. Qiao, L. Zhou, B. Wang, J. Zhang, C. Chen, J. Li, X. Xiao, Adeno-associated virus serotype 8 efficiently delivers genes to muscle and heart. *Nat. Biotechnol.* **23**, 321–328 (2005).

45. H. T. McMahon, E. Boucrot, Molecular mechanism and physiological functions of clathrin-mediated endocytosis. *Nat. Rev. Mol. Cell Biol.* **12**, 517–533 (2011).

46. J. Rejman, V. Oberle, I. S. Zuhorn, D. Hoekstra, Size-dependent internalization of particles via the pathways of clathrin- and caveolae-mediated endocytosis. *Biochem. J.* **377**, 159–169 (2004).

47. S. Alexander, Adsorption of chain molecules with a polar head a scaling description. *J. Phys. France* **38**, 983–987 (1977).

48. P. G. de Gennes, Conformations of polymers attached to an interface. *Macromolecules* **13**, 1069–1075 (1980).

49. S. Watanabe, K. Hayashi, K. Toh, H. J. Kim, X. Liu, H. Chaya, S. Fukushima, K. Katsushima, Y. Kondo, S. Uchida, S. Ogura, T. Nomoto, H. Takemoto, H. Cabral, H. Kinoh, H. Y. Tanaka, M. R. Kano, Y. Matsumoto, H. Fukuhara, S. Uchida, M. Nangaku, K. Osada, N. Nishiyama, K. Miyata, K. Kataoka, In vivo rendezvous of small nucleic acid drugs with charge-matched block catiomers to target cancers. *Nat. Commun.* **10**, 1894 (2019).

50. A. Dirisala, S. Uchida, T. A. Tockary, N. Yoshinaga, J. Li, S. Osawa, L. Gorantla, S. Fukushima, K. Osada, K. Kataoka, Precise tuning of disulphide crosslinking in mRNA polyplex micelles for optimising extracellular and intracellular nuclease tolerability. *J. Drug Target.* **27**, 670–680 (2019).

51. O. F. Mutaf, A. Kishimura, Y. Mochida, A. Kim, K. Kataoka, Induction of secondary structure through micellization of an oppositely charged pair of homochiral block- and homopolypeptides in an aqueous medium. *Macromol. Rapid Commun.* **36**, 1958–1964 (2015).

52. G. L. Kenausis, J. Vörös, D. L. Elbert, N. Huang, R. Hofer, L. Ruiz-Taylor, M. Textor, J. A. Hubbell, N. D. Spencer, Poly($_L$-lysine)-*g*-poly(ethylene glycol) layers on metal oxide surfaces: Attachment mechanism and effects of polymer architecture on resistance to protein adsorption. *J. Phys. Chem. B* **104**, 3298–3309 (2000).